Accurate ab-Initio-Based Single-Sheeted DMBE Potential-Energy Surface for Ground-State N2O

ARTICLE *in* THE JOURNAL OF PHYSICAL CHEMISTRY A · APRIL 2012

Impact Factor: 2.69 · DOI: 10.1021/jp302173h · Source: PubMed

2 AUTHORS:

Jing Li
University of Coimbra
14 PUBLICATIONS **44** CITATIONS
SEE PROFILE

Antonio J. C. Varandas
University of Coimbra
382 PUBLICATIONS **6,733** CITATIONS
SEE PROFILE

THE JOURNAL OF PHYSICAL CHEMISTRY A

Article

pubs.acs.org/JPCA

Accurate ab-Initio-Based Single-Sheeted DMBE Potential-Energy Surface for Ground-State N_2O

Jing Li and António J. C. Varandas*

Departamento de Química, Universidade de Coimbra, 3004-535 Coimbra, Portugal

Supporting Information

ABSTRACT: A global accurate double-many-body expansion potential-energy surface is reported for the electronic ground state of N_2O. The new form is shown to accurately mimic the ab-initio points calculated at the multireference configuration interaction level using the aug-cc-pVTZ basis set and the full-valence-complete-active-space wave function as reference. To improve the calculated raw energies, they have been extrapolated to the completed basis set limit and most importantly to the full configuration-interaction limit by correcting semiempirically the calculated dynamical correlation with the double-many-body expansion-scaled external correlation method. The topographical features of the novel potential-energy surface were examined in detail and compared with those of other potential functions available in the literature. Good agreement with the experimental data is observed.

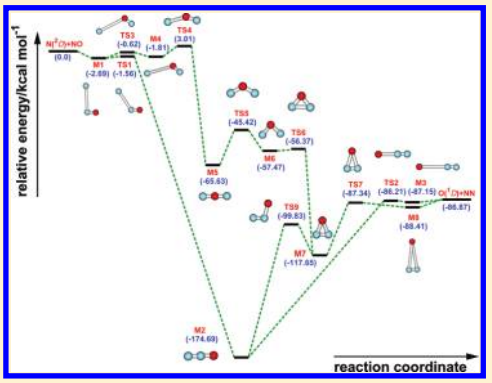

1. INTRODUCTION

Nitrous oxide (N_2O) is an extremely important species in atmospheric chemistry. Emission of N_2O is currently the single most important ozone-depleting process and expected to remain the largest throughout the 21st century.[1] Among the main three dissociation processes of the title system,

$$N_2O(X^1\Sigma^+) \rightarrow O(^1D) + N_2(X^1\Sigma_g^+) \quad (1)$$

$$\rightarrow N(^2D) + NO(X^2\Pi) \quad (2)$$

$$\rightarrow O(^3P) + N_2(X^1\Sigma_g^+) \quad (3)$$

process 1 is the main loss mechanism and therefore has a significant impact on the chemistry of the atmosphere, being studied in great detail experimentally as well as theoretically. Process 2 can also take place in the ground electronic state of N_2O, but only a few theoretical studies and several experimental kinetic ones are available. Dissociation of N_2O via channel 3 to singlet and triplet states is forbidden under $C_{\infty v}$ symmetry but becomes allowed under C_s symmetry and may be significant due to vibrational averaging.

The nitrous oxide molecule has been an important subject of study in a number of scientific fields such as life sciences,[2] earth sciences,[3] atmospheric sciences,[4] and fuel industry.[5] It has also been the subject of various theoretical and experimental studies.[6−8] Theoretical studies of nitrous oxide date back to the two-dimensional potential-energy surfaces (PESs) calculated by Brown et al.[9] with the NN bond length kept fixed at the experimental value of 2.13199 a_0 and used by Johnson et al.[10] in dynamics calculations. In the same year, Nakamura and Kato[11] calculated the spin-forbidden predissociation reaction of N_2O using a PES of the double-many-body-expansion (DMBE[12−14]) family fitted to their own ab-initio calculations for the singlet and triplet surfaces that are coupled by spin−orbit terms. Subsequently, González et al.[15] made an extensive theoretical study of the $N(^2D) + NO(X^2\Pi) \rightarrow O(^1D) + N_2(X^1\Sigma_g^+)$ exothermic reaction on its lowest $^1A'$ PES and found several minima and transition states along the different minimum energy paths (MEPs) connecting reactants and products. Improved electronic structure calculations were later carried out by Daud et al.[16] using the complete-active-space self-consistent field (CASSCF) and multireference configuration-interaction (MRCI) methods, still keeping the NN bond fixed at the equilibrium value. At about the same time, Nanbu and Johnson[17] reported full three-dimensional PESs and utilized them for dynamics calculations. Recently, Schinke[18] calculated the ground-state and exited-state potential-energy surfaces and performed dynamics calculations. Most recently, Defazio et al.[19] reported spin−orbit and Renner−Teller quantum dynamics of the spin-forbidden quenching reaction $O(^1D) + N_2(X^1\Sigma_g^+) \rightarrow O(^3P) + N_2(X^1\Sigma_g^+)$ on the N_2O $\tilde{X}^1A'$, $\tilde{a}^3A''$, and $\tilde{b}^3A'$ PESs. For the ground electronic state of the N_2O molecule, the majority of structural studies focus on its global minimum. Thus, the design of the grid of points chosen to calculate the PES via ab-initio calculations is usually focused onto the vicinity of the potential well of the linear $C_{\infty v}$ isomer. Indeed, as far as we are aware, no work toward obtaining a global potential-energy surface for the ground state of N_2O has been reported. Therefore, there is a need for a realistic global potential-energy surface of nitrous oxide, which covers a large angular area and is sufficiently accurate for studies of reaction dynamics and chemical kinetics. Thus, we report in the present

Received: March 6, 2012
Revised: April 11, 2012
Published: April 11, 2012

work a realistic global PES for ground-state N_2O via DMBE[12−14] theory which is calibrated from 809 ab-initio points calculated at the multireference configuration interaction (MRCI)[20] level of theory using the full-valence-complete-active-space (FVCAS)[21] wave function as reference and Dunning's[22,23] aug-cc-pV*T*Z (AV*T*Z) basis set. The ab-initio energies calculated in this way have been subsequently corrected using the double-many-body expansion-scaled external correlation method (DMBE-SEC)[24] method to extrapolate them to the complete configuration-interaction limit. As usual in DMBE theory, the PES so obtained (hereinafter referred to as DMBE PES) shows the correct long-range behavior at all dissociation channels while providing a realistic representation of the surface features at all interatomic separations.

The paper is organized as follows. Section 2 reports the ab-initio calculations here performed, while section 3 surveys the DMBE formalism. The topographical features of the DMBE PES are discussed in section 4. Section 5 gathers the concluding remarks.

2. AB-INITIO CALCULATIONS

Ab-initio calculations have been carried out at the MRCI level using the FVCAS wave function as reference. The AV*T*Z basis set of Dunning has been employed, with the calculations performed using the Molpro[25] package. A grid of 809 ab-initio points has been chosen to map the PES over the O−N_2 region defined by $1.5 \le R_{N_2}/a_0 \le 3.5$, $1.0 \le r_{O-N_2}/a_0 \le 10.0$, and $0 \le \gamma/\text{deg} \le 90$. For the N−NO interactions, a grid defined by $1.5 \le R_{NO}/a_0 \le 3.5$, $1.0 \le r_{N-NO}/a_0 \le 10.0$, and $0 \le \gamma/\text{deg} \le 180$ has been chosen. For both channels, r, R, and γ are the atom−diatom Jacobi coordinates.

To account for electronic excitations beyond singles and doubles and, most importantly, for the incompleteness of the basis set, the calculated ab-initio energies have been subsequently corrected using the DMBE-SEC method. Thus, the total DMBE-SEC interaction energy is written as

$$V(\mathbf{R}) = V_{\text{FVCAS}}(\mathbf{R}) + V_{\text{SEC}}(\mathbf{R}) \tag{4}$$

where

$$V_{\text{FVCAS}}(\mathbf{R}) = \sum_{\text{AB}} V^{(2)}_{\text{AB,FVCAS}}(R_{\text{AB}}) + V^{(3)}_{\text{ABC,FVCAS}}(\mathbf{R}) \tag{5}$$

$$V_{\text{SEC}}(\mathbf{R}) = \sum_{\text{AB}} V^{(2)}_{\text{AB,SEC}}(R_{\text{AB}}) + V^{(3)}_{\text{ABC,SEC}}(\mathbf{R}) \tag{6}$$

where $\mathbf{R} = \{R_{\text{AB}},R_{\text{BC}},R_{\text{AC}}\}$ is a collective variable of all internuclear distances. Explicitly, expansion of the two terms in eq 6 assumes the form

$$V^{(2)}_{\text{AB,SEC}}(R_{\text{AB}}) = \frac{V^{(2)}_{\text{AB,FVCAS-CISD}}(R_{\text{AB}}) - V^{(2)}_{\text{AB,FVCAS}}(R_{\text{AB}})}{F^{(2)}_{\text{AB}}} \tag{7}$$

$$V^{(3)}_{\text{ABC,SEC}}(\mathbf{R}) = \frac{V^{(3)}_{\text{AB,FVCAS-CISD}}(\mathbf{R}) - V^{(3)}_{\text{ABC,FVCAS}}(\mathbf{R})}{F^{(3)}_{\text{ABC}}} \tag{8}$$

Following previous work,[24] $F^{(2)}_{\text{AB}}$ in eq 7 is chosen to reproduce the bond dissociation energy of the corresponding AB diatom while $F^{(3)}_{\text{ABC}}$ in eq 8 is estimated as the average of the three two-body F factors. Such a procedure leads to the following results for the AV*T*Z basis set: $F^{(2)}_{\text{NN}} = 0.3532$, $F^{(2)}_{\text{NO}} = 0.6532$, and $F^{(3)}_{\text{ONN}} = 0.5532$. Not surprisingly, due to triple-ζ basis sets being known to recover only a modest fraction of the calculated dynamical correlation, the scaling factor for N_2 turns out to be smaller than 0.5. Although this could, in principle, question the validity of the approach, it turns out that the results to be presented later do not appear to show any undesirable misprediction. Since the use of a larger basis set would make the present work much more expensive, we are content with those here presented.

3. DOUBLE-MANY-BODY-EXPANSION POTENTIAL-ENERGY SURFACE

The title system has the following dissociation scheme

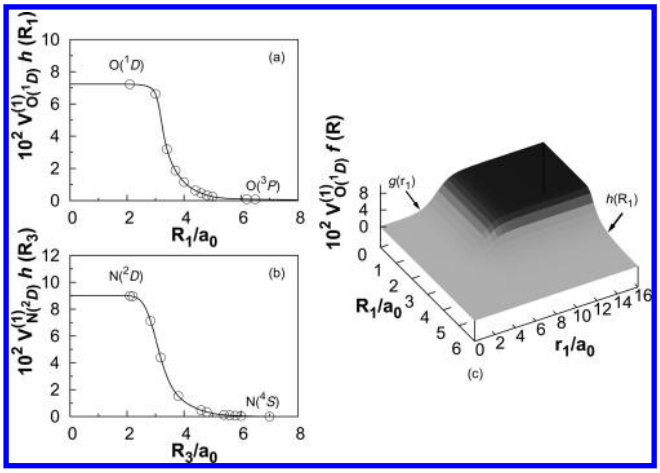

Figure 1. Switching function used to model the pseudo-one-body energy terms in the single-sheeted N_2O DMBE PES of the present work. (a) Fit of the $h(R_1)$ switching form to the ab-initio points calculated for the O + N_2 configuration as a function of the N−N distance (R_1). (b) Fit of $h(R_3)$ for the N + NO configuration as a function of the N−O distance (R_3). (c) Perspective view of the global switching function $f_1(\mathbf{R})$ for oxygen.

$$N_2O(^1A') \rightarrow N_2(X^1\Sigma_g^+) + O(^1D) \tag{9}$$

$$\rightarrow NO(X\,^2\Pi) + N(^2D) \tag{10}$$

Since the diatomic molecules $NO(X\ ^2\Pi)$ and $N_2(X^1\Sigma_g^+)$ dissociate to their ground-state atoms [i.e., $N(^4S)$ and $O(^3P)$] but the excited-state atoms [i.e., $N(^2D)$ and $O(^1D)$] appear in the above two channels, it is unavoidable to use switching functions in order to obtain an approximate representation of the actual multisheeted PES by a single-sheeted one. Such a procedure has been proposed by Murrell and Carter,[26] who applied it in the construction of an approximate PES for the ground-state H_2O. Accordingly, in 2000 González et al.[15] made a detailed study of the reaction

$$N(^2D) + NO(X\,^2\Pi) \rightarrow O(^1D) + N_2(X\,^1\Sigma_g^+)$$

using the switching function for the oxygen and nitrogen atoms. Although the Murrell−Carter switching forms (also utilized by González et al.[15]) can ensure the correct asymptotic limit, they fail to warrant a unique value for the energy at the geometries of the system where three atoms are far away from each other. Such inconsistency prompted us to obtain a single-sheeted function capable of mimicking both the $N(^2D)$ + $NO(X\ ^2\Pi)$

dx.doi.org/10.1021/jp302173h | J. Phys. Chem. A 2012, 116, 4646−4656

Table 1. Equilibrium Geometries (in Angstroms), Vibrational Frequencies (cm^{-1}), and Dissociation Energies (kcal mol^{-1}) of N_2 and NO

	$N_2(X^1\Sigma_g^+)$			$NO(X^2\Pi)$			ΔE^c	
method	R_e	D_e	w_e	R_e	D_e	w_e	$N(^4S-^2D)$	$O(^3P-^1D)$
DMBE PES[a]	1.1038	228.47	2331.6	1.1563	152.56	1884.4	56.34	45.39
CASSCF/AVTZ[b]	1.1056	212.04	2330.6	1.1558	130.10	1880.2	69.97	51.42
MRCI(Q)/AVTZ[b]	1.1056	219.23	2322.3	1.1585	144.52	1882.1	58.68	46.73
CASSCF/6-311G(2d)[15]	1.1056	210.36	2334.6	1.1609	128.23	1878.0	66.00	51.51
CASPT2/6-311G(2d)[15]	1.1034	212.55	2316.7	1.1598	140.73	1857.9	62.07	48.65
exp.[50,51]	1.0977	228.41	2358.6	1.1508	152.53	1904.2	54.96	45.37

[a]This work. From the potential-energy curves fitted to MRCI/AVTZ energies. [b]This work. From ab-initio points at CASSCF and MRCI(Q) levels of theory. [c]Energy difference between $N(^4S)$ to $N(^2D)$ and $O(^3P)$ to $O(^1D)$.

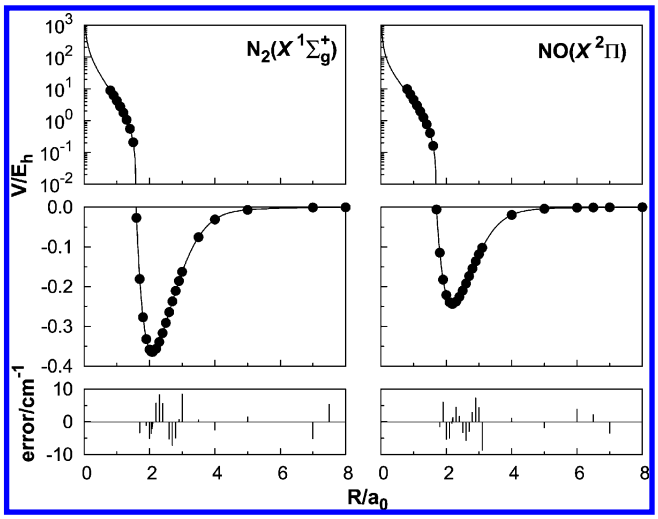

Figure 2. Potential-energy curve for $N_2(X^1\Sigma_g^+)$ and $NO(X^2\Pi)$ and the differences between the energies predicted from the fit and the actual ab-initio energies.

Table 2. Numerical Values for NO Dipole and Quadrupole Moments and NN Quadrupole Moment

	D_{NO}	Q_{NO}	Q_{NN}
Q_∞/ea_0^2		0.449421	0.0
M_6/ea_0^8		3500	3500
R_{ref}/a_0	3.32461	5.17897	4.9296
D_M[a]	−0.234954	−0.0594638	−0.150932
a_1/a_0^{-1}	−0.161567	0.749951	0.879603
a_2/a_0^{-2}	−0.738644	0.272525	0.288471
a_3/a_0^{-3}	0.471858	0.0132849	0.0189779
b_1/a_0^{-1}		2.50415	2.5508
b_1/a_0^{-2}	0.462051	0.502533	0.54759
b_1/a_0^{-3}	0.18244	0.0196438	0.0170144

[a]The units are ea_0 for D_{NO} and ea_0^2 for Q_{NO} and Q_{NN}.

and the $O(^1D) + N_2(X^1\Sigma_g^+)$ dissociation limits using a variant of a switching function previously developed in our group[27] assuming the form

$$h_i(\mathbf{R}_i) = \frac{1}{4}\sum_{m=1}^{2}\{1 - \tanh[\alpha_m(R_i - R_i^{m0}) + \beta_m(R_i - R_i^{m1})^3]\},$$
$$i = 1, 2, 3 \quad (11)$$

where i = 1, 2, and 3 are indexes employed to label the O, N_a, and N_b atoms, respectively, R_1, R_2, and R_3 represent the N_a-N_b, N_a-O, and N_b-O distances, respectively, while a and b

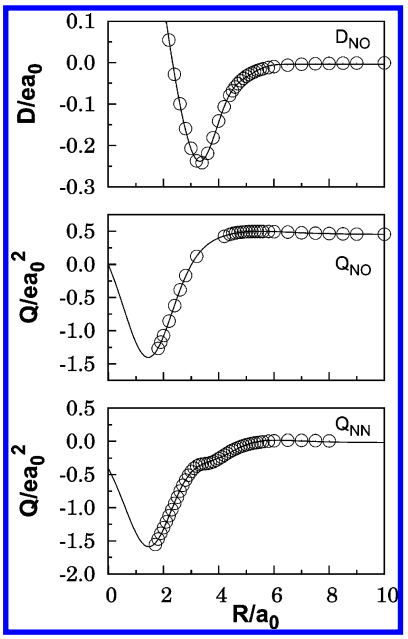

Figure 3. Variation of the NO dipole and quadrupole moments and NN quadrupole moment with internuclear distance.

Table 3. Stratified Root-Mean-Square Deviations (in kcal mol^{-1}) of the DMBE PES

energy[a]	N^b	max dev[c]	rmsd	$N^d_{>rmsd}$
10	76	0.478	0.187	19
20	93	1.297	0.268	19
30	106	1.473	0.344	17
40	109	1.473	0.371	18
50	116	1.473	0.400	20
60	121	1.473	0.410	22
70	136	2.312	0.507	26
80	161	4.103	0.798	32
90	189	4.103	0.841	39
100	243	4.103	0.843	55
200	617	4.142	0.916	159
300	802	4.142	0.932	202
400	807	4.142	0.936	204
500	809	4.142	0.940	204

[a]The units of energy and rmsd are kcal mol^{-1}. [b]Number of points in the indicated energy range. [c]Maximum deviation up to the indicated energy range. [d]Number of points with an energy deviation larger than the rmsd.

dx.doi.org/10.1021/jp302173h | J. Phys. Chem. A 2012, 116, 4646−4656

distinguish the two identical N atoms. In turn, α_m and β_m are parameters to be calibrated from a least-squares fit to an extra set of 15 AVTZ points that control the $O(^1D)-O(^3P)$ decay as the N_a-N_b distance increases for O + N_2 configurations, as shown in Figure 1a, and another set of 23 AVTZ points that control the $N(^2D)-N(^4S)$ decay as the N_b-O distance increases for the N_a + N_bO configurations, as shown in Figure 1b. Because N_a and N_b are indistinguishable, the same set of parameters in the switching function is attributed to nitrogen atoms *a* and *b*. As a check to the fit, we observe that at the diatomic equilibrium bond length the switching function becomes smaller than 10^{-6}, thus warranting the correct energetics at the $N(^2D)$ + $NO(X\ ^2\Pi)$ and $O(^1D)$ + $N_2(X^1\Sigma_g^+)$ asymptotes. To get a smooth three-body energy term, we further choose to multiply eq 11 by an amplitude function that annihilates eq 11 at short range (short $O-N_2$ and N−NO distances)

$$g_i(\mathbf{r}_i) = \frac{1}{2}\{1 + \tanh[\alpha(r_i - r_i^0)]\},\ i = 1, 2, 3 \tag{12}$$

where $\mathbf{r}_1$ is the distance of the O atom to the center of mass of N_2. A word is necessary at this point to clarify the notation. The indexes (*i*,*j*,*k*) number atoms (say, 1 for O and 2 and 3 for N), and r_i represents the Jacobi coordinate separating atom *i* from the center of mass of diatom *jk* whose bond distance is itself denoted by R_i. The final switching function then assumes the form

$$f_i(\mathbf{R}) = g_i(r_i)h_i(R_i),\ i = 1, 2, 3 \tag{13}$$

with the parameters of $g(r_i)$ being chosen such as to guarantee that its main effect occurs for $O-N_2$ and N−NO distances larger than 8 a_0 or so, as illustrated in Figure 1c. All numerical values of the parameters in eq 13 are collected in Table 1.

Within the framework of DMBE theory, the single-sheeted PES assumes the form

$$\begin{aligned} V(\mathbf{R}) = {} & V^{(1)}_{O(^1D)} f_1(\mathbf{R}) + V^{(1)}_{N_a(^2D)} f_2(\mathbf{R}) + V^{(1)}_{N_b(^2D)} f_3(\mathbf{R}) \\ & + \sum_{i=1}^{3} [V^{(2)}_{EHF}(R_i) + V^{(2)}_{dc}(R_i)] + V^{(3)}_{EHF}(\mathbf{R}) \\ & + V^{(3)}_{dc}(\mathbf{R}) \end{aligned} \tag{14}$$

In the one-body term $V^{(1)}_{O(^1D)}$ represents the energy difference between the ^1D and the ^3P states of atomic oxygen, $V^{(1)}_{O(^1D)}$ = 0.0723399 E_h, and $f_1(\mathbf{R})$ is the switching function used to warrant the correct behavior at the $N_2(X^1\Sigma_g^+)$ + $O(^1D)$ dissociation limits. Similarly, $V^{(1)}_{Na(^2D)}$ and $V^{(1)}_{Nb(^2D)}$ represent the energy difference between the $N(^2D)$ and $N(^4S)$ states: $V^{(1)}_{Na(^2D)}$, $V^{(1)}_{Nb(^2D)}$ = 0.0898679 E_h. Correspondingly, $f_2(\mathbf{R})$ and $f_3(\mathbf{R})$ are the switching functions that warrant the correct behavior at the $NO(X\ ^2\Pi)$ + $N(^2D)$ dissociation limit. Table 1 compares the calculated energy differences for atomic oxygen and nitrogen with the experimental results. As seen, the results of the DMBE PES give a very good overall behavior of such attributes, improving significantly the energy differences with respect to ab-initio results. The energy differences for nitrogen and oxygen with respect to the experimental data are seen to be of 1.38 and 0.02 kcal mol^{-1} (respectively), thus in very good agreement with the experimental counterpart. Of course, this is an essential requirement for construction of a realistic PES to be used for dynamics and kinetics studies.

Note that we used the switching functions for O, N_a, and N_b separately. In fact, for the title system, when the oxygen atom is in the $O(^1D)$ excited state, the nitrogen atom must decay to $N(^4S)$, because the N_2 fragment is on its ground singlet state. This behavior is well described by our switching functions, since the oxygen atom is in the $O(^1D)$ excited state for large intermolecular distances of r_{O-N_2} and short N−N bond distances, with both N_a and N_b decaying to $N(^4S)$ with growing N−O distance. Of course, an accurate representation of the PES would require at least a double-sheeted representation of the PES, i.e., $N(^4S)$ + $N(^4S)$ + $O(^1D)$ and $N(^2D)$ + $N(^4S)$ + $O(^3P)$. However, we expect the above approximate single-sheeted representation to provide a realistic description of the lowest adiabatic singlet-state PES for the title molecule.

As usual in DMBE theory, the two-body and three-body energy terms will be split into two contributions: the extended Hartree−Fock (EHF) and dynamical correlation (dc) energies. The following subsections give a brief description of the various energy terms, with the reader being addressed to refs 27 and 28 and references therein for details.

3.1. Two-Body Energy Terms. For the diatomic potential-energy curves, we employ the extended Hartree−Fock approximate correlation energy method, including the united atom limit (EHFACE2U),[29] which shows the correct behavior at the asymptotes $R \to 0$ and $R \to \infty$. In turn, the EHF energy part of diatomic curve assumes the form

$$V_{EHF}(R) = -\frac{D}{R}\left(1 + \sum_{i=1}^{n} a_i r^i\right)\exp(-\gamma r) \tag{15}$$

where $\gamma = \gamma_0[1 + \gamma_1 \tanh(\gamma_2 r)]$ and $r = R - R_e$ is the displacement from the equilibrium diatomic geometry. In turn, the dc energy contribution is written as[30]

$$V_{dc}(R) = -\sum_{n=6,8,10} C_n \chi_n(R) R^{-n} \tag{16}$$

In the present work, the potential-energy curves for both $NO(X\ ^2\Pi)$ and $N_2(X^1\Sigma_g^+)$ are modeled from our own calculated ab-initio energies and experimental dissociation energy[31,32] as implied by the DMBE-SEC[24] method. As shown in Figure 2, both potential curves mimic accurately the calculated ab-initio energies. Equilibrium geometries, vibrational frequencies, and dissociation energies are also collected in Table 1. As seen, the results at the MRCI(Q) level of theory are closer to the experimental values, although the tendency is not so clear when considering the vibrational frequencies. The increase in accuracy of the dissociation energy of the diatomic when the raw ab-initio points are corrected by scaling[33] the dynamical correlation as in the DMBE-SEC[24] method is remarkable. The numerical values of all parameters for both diatomic curves are gathered in Table 2 of the Supporting Information (the number of significant figures in the tabulated Supporting Information may appear be excessive in some cases but is given for convenience in reproducing the data).

3.2. Three-Body Energy Terms. *3.2.1. Three-Body Dynamical Correlation Energy.* The three-body dc energy assumes the usual form of a summation in inverse powers of the fragment separation distances[28]

$$V^{(3)}_{dc} = -\sum_i \sum_n f_i(\mathbf{R}) \chi_n(r_i) C_n^{(i)}(R_i, \theta_i) r_i^{-n} \tag{17}$$

dx.doi.org/10.1021/jp302173h | J. Phys. Chem. A 2012, 116, 4646−4656

Table 4. Minima of N_2O DMBE PES

feature	method	E^c/kcal mol^{-1}	R_{NN}/Å	R_{NO}/Å	α^d	ω_1	ω_2	ω_3
$C_{\infty v}$								
M2	DMBE[a]	−174.69, −89.63	1.1399	1.1928	180.0	2251.3	1314.1	453.6
	MRCI(Q)/AVTZ[b]	−170.00, −82.55	1.1322	1.1882	180.0	2283.9	1298.8	600.3
	CASPT2/6-311G(2d)[15]	−170.10, −84.85	1.1355	1.1947	180.0	2223.7	1269.6	589.5
	González et al.[15]	−170.90	1.1326	1.1999	180.0	2216.5	1250.2	589.7
	Schinke[18]	−85.63	1.1315	1.1897	180.0			
	exp.[48]	−172.50, −87.25	1.1282	1.1842	180.0	2223.7	1276.5	589.2
$D_{\infty h}$								
M5	DMBE[a]	−65.63	2.4175	1.2087	180.0	1726.6	1059.3	508.4
	MRCI(Q)/AVTZ[b]	−63.25	2.4361	1.2180	180.0	1722.8	1079.6	432.2
	CASPT2/6-311G(2d)[15]	−62.71	2.4256	1.2128	180.0	1695.7	1056.4	434.4
	González et al.[15]	−63.78	2.3237	1.1618	180.0	2041.8	894.1	245.3
C_{2v}								
M6	DMBE[a]	−57.47	1.8520	1.3097	89.5	1222.9	460.1	1037.5
	CASPT2/6-311G(2d)[15]	−46.72	1.7416	1.3547	80.0	1104.8	187.0	890.8
M7	DMBE PES[a]	−117.65	1.1891	1.5145	46.2	2047.0	857.6	235.2
	MRCI(Q)/AVTZ[b]	−102.86	1.2037	1.5492	45.7	1763.3	740.1	267.8
	CASPT2/6-311G(2d)[15]	−103.45	1.2054	1.5487	45.3	1731.0	757.2	303.2
	González et al.[15]	−104.60	1.1558	1.5887	42.7	1745.7	913.7	682.5
M8	DMBE[a]	−88.41	1.1050	3.6426	17.2	2320.8	105.7	40.4
	CASPT2/6-311G(2d)[15]	−85.89	1.1061	2.9785	21.4	2010.3	46.0	299.4
	González et al.[15]	−86.31	1.1170	2.7413	23.5	2153.4	168.9	146.1
C_s								
M1	DMBE[a]	−2.69	3.5776	1.1611	93.0	1823.5	60.2	32.5
	CASPT2/6-311G(2d)[15]	−1.37	3.2166	1.1597	93.4	1801.7	43.9	12.3
	González et al.[15]	−0.65	3.3471	1.1590	158.4	1847.7	64.3	23.0
M3	DMBE PES[a]	−87.15	1.1071	3.9188	179.6	2303.0	53.0	36.9
	CASPT2/6-311G(2d)[15]	−86.10						
	González et al.[15]	−87.37	1.1109	2.8191	131.3	2306.8	184.2	103.8
M4	DMBE[a]	−1.81	3.6426	2.7375	134.6	1869.4	95.3	83.5
	CASPT2/6-311G(2d)[15]	−1.58	3.3416	2.6062	120.2	1854.3	141.6	78.8
	González et al.[15]	−5.05	3.1981	2.7543	102.1	1855.9	293.4	232.2

[a]This work. From fit to DMBE-SEC energies resulting from MRCI(Q)/AVTZ calculations. [b]This work. Stationary points obtained through optimization at the MRCI/AVTZ level of theory. [c]Energies relative to $N(^2D)$ + NO and $O(^1D)$ + N_2 asymptotes, from left-hand side to right-hand side, respectively. [d]α is the angle ∠NON of C_{2v}, $D_{\infty h}$, and NON (C_s) structures, or ∠NNO otherwise.

where the first summation runs over all atom−diatom interactions ($i \equiv$ A−BC), R_i is the diatomic internuclear distance, r_i is the separation between atom A and the center-of-mass separation of the BC diatom, and θ_i is the angle between these two vectors (see Figure 1 of ref 34). In turn, $f_i(\mathbf{R}) = (1/2)\{1 - \tanh[\xi(\eta R_i - R_j - R_k)]\}$ is a convenient switching function. Following recent work,[27] we fixed $\eta = 6$ and $\xi = 1.0a_0^{-1}$, while the damping function $\chi_n(r_i)$ takes the form employed elsewhere.[28,27] All numerical values of the parameters in eq 17 are given in Table 3 in the Supporting Information, while their internuclear dependences are displayed in Figure 1.

3.2.2. Three-Body Electrostatic Energy. The electrostatic energy is due to the interaction of the quadrupole and higher permanent electric moments of $O(^1D)$ and $N(^2D)$ with the dipole and higher ones of $N_2(X^1\Sigma_g^+)$ and $NO(X\ ^2\Pi)$. In the present work, we considered the interactions of the oxygen quadrupole with the nitric oxide dipole and quadrupole moments and nitrogen quadrupole with the N_2 dipole and quadrupole moments. Following previous work,[35−37] the electrostatic energy is written as

$$V_{ele}^{(3)} = f(\mathbf{R})\{C_4(R, r)A_{DQ}(\theta_a, \theta, \phi_{ab})r^{-4} + C_5(R, r)A_{QQ}(\theta_a, \theta, \phi_{ab})r^{-5}\} \quad (18)$$

where $f(\mathbf{R})$, R, r, and θ have the same meaning as in section 3.2.1, θ_a is the angle that defines the atomic quadrupole orientation, and ϕ_{ab} is the corresponding dihedral angle. Since the N_2 permanent electric dipole moment $D_{NN}(R)$ is 0, the coefficients $C_4(R,r)$ and $C_5(R,r)$ are given by

$$C_4(R, r) = \frac{3}{2}Q_N D_{NO}(R)\chi_4(r)$$

$$C_5(R, r) = \frac{3}{4}\{Q_N Q_{NO}(R) + Q_O Q_{NN}(R)\}\chi_5(r) \quad (19)$$

where $D_{NO}(R)$ and $Q_{NO}(R)$ are the permanent electric dipole and quadruple moments of NO and $Q_{NN}(R)$ is the quadruple moment of NN. Q_N and Q_O are the quadruple moments of the nitrogen and oxygen atoms. The functional form of the angular variations of A_{DQ} and A_{QQ} take the expressions employed in previous work[35,37,38] based on the classical-optimized-quadruple (COQ) model.[39−43]

The analytical expression for the NO dipole has been obtained by fitting our own ab-initio results to the form[44]

$$D(R) = D_M\left(1 + \sum_{i=1}^{3} a_i r^i\right)\exp\left(-a_1 r - \sum_{i=2}^{3} b_i r^i\right) \quad (20)$$

dx.doi.org/10.1021/jp302173h | J. Phys. Chem. A 2012, 116, 4646−4656

Table 5. Transition States of N_2O DMBE PES

feature	ref	E^c/kcal mol^{-1}	R_{NN}/Å	R_{NO}/Å	α^d	ω_1	ω_2	ω_3
$C_{\infty v}$								
TS2	DMBE[a]	−86.21	1.1045	2.3487	180.0	2350.7	136.4	235.5i
	CASPT2/6-311G(2d)[15]	−88.20						
	González et al.[15]	−86.4	1.1027	2.3869	150.6	2335.5	122.8	195.3i
C_s								
TS1	DMBE[a]	−1.56	3.0486	1.1489	124.5	1913.2	84.33	157.5i
	González et al.[15]	−0.46	2.8792	1.1554	140.7	1815.6	103.7	94.6i
TS3	DMBE[a]	−0.62	4.3557	1.1611	113.3	1820.3	48.9	54.3i
	González et al.[15]	−0.13	3.7490	1.1574	93.6	1852.2	38.1	70.1i
TS4	DMBE[a]	3.01	2.8994	2.5354	96.3	1738.1	225.3	254.5i
	CASPT2/6-311G(2d)[15]	1.90	3.0965	2.0914	140.8	1825.6	195.7	509.6i
	González et al.[15]	1.91	2.9979	2.1367	129.9	1709.8	201.6	418.0i
TS9	DMBE[a]	−99.83	1.1743	1.4240	100.3	1664.8	751.3	786.1i
	MRCI(Q)/AVTZ[b]	−89.64	1.1214	1.4208	102.1	1802.3	682.5	724.3i
	CASPT2/6-311G(2d)[15]	−88.65	1.1452	1.4122	101.4	1856.1	549.0	541.7i
	González et al.[15]	−90.46	1.1347	1.4029	97.6	1986.3	810.2	744.7i
C_{2v}								
TS5	DMBE[a]	−45.42	2.2419	1.3055	118.3	960.2	504.4i	1256.6
	MRCI(Q)/AVTZ[b]	−42.48	2.2559	1.3133	118.3	996.6	590.4i	1139.3
	CASPT2/6-311G(2d)[15]	−38.79	2.2650	1.3205	118.1	973.8	570.2i	1117.8
TS6	DMBE[a]	−56.37	1.7986	1.3889	80.7	961.6	262.7i	795.6
	MRCI(Q)/AVTZ[b]	−50.75	1.7965	1.3823	81.0	1042.3	311.6i	892.3
	CASPT2/6-311G(2d)[15]	−46.59	1.7950	1.3465	83.6	1117.5	302.7i	939.9
	González et al.[15]	−45.70	1.7643	1.3171	85.3	1254.0	518.6i	1018.1
TS7	DMBE[a]	−87.34	1.1077	2.2572	28.4	2312.1	232.3i	181.1
	MRCI(Q)/AVTZ[b]	−83.51	1.1122	2.1199	30.0	2155.4	465.3i	282.6
	CASPT2/6-311G(2d)[15]	−83.05	1.1176	2.1043	30.8	2025.9	336.8i	286.8
	González et al.[15]	−82.49	1.1100	2.1379	30.1	2174.7	385.6i	410.1

[a]This work. From fit to DMBE-SEC energies resulting from calculated MRCI(Q)/AVTZ points. [b]This work. Stationary points calculated by optimization at the MRCI/AVTZ level of theory. [c]Energies given relative to N(^2D) + NO asymptote. [d]α is the angle ∠NON for C_{2v} and $D_{\infty h}$ and NON (C_s) structure, or ∠NNO otherwise.

where $r = R - R_{ref}$ and R_{ref} is the reference distance corresponding to the maximum in the $D(R)$ curve. In turn, the variation of the NO and NN quadrupole moments with the internuclear distance as approximated by their z components has been modeled by[43]

$$Q(R) = D_M\left(1 + \sum_{i=1}^{3} a_i r^i\right)\exp\left(-\sum_{i=1}^{3} b_i r^i\right) + Q_\infty + \chi_8(R)\frac{M^6}{R^6} \quad (21)$$

where $r = R - R_{ref}$ with R_{ref} is the reference distance corresponding to the maximum in the $Q(R)$ curve. Q_∞ is the value of the quadrupole limit. The parameters in eqs 20 and 21 are collected in Table 2, while a graphical view of the modeled functions can be seen in Figure 3.

3.2.3. Three-Body Extended Hartree–Fock Energy. The total three-body energy can be obtained, for a given triatomic geometry by removing the sum of the one-body and two-body energy terms from the corresponding DMBE-SEC interaction energies in eq 14. Subsequently, by subtracting both the three-body dc energy part described in eq 17 and the three-body electrostatic energy in eq 18 from the total three-body energy one obtains the three-body EHF energy. This can now be suitably represented by the following three-body distributed polynomial[45] form

$$V_{EHF}^{(3)} = \sum_{j=1}^{5} P^j(Q_1, Q_2, Q_3) \times \prod_{i=1}^{3}\{1 - \tanh[\gamma_i^j(R_i - R_i^{j,ref})]\} \quad (22)$$

where $P^j(Q_1,Q_2,Q_3)$ is the jth polynomial up to six order in the symmetry coordinates which are defined as

$$\begin{pmatrix} Q_1 \\ Q_2 \\ Q_3 \end{pmatrix} = \begin{pmatrix} \sqrt{1/3} & \sqrt{1/3} & \sqrt{1/3} \\ 0 & \sqrt{1/2} & -\sqrt{1/2} \\ \sqrt{2/3} & -\sqrt{1/6} & -\sqrt{1/6} \end{pmatrix}\begin{pmatrix} R_1 - R_1^{j,ref} \\ R_2 - R_2^{j,ref} \\ R_3 - R_3^{j,ref} \end{pmatrix} \quad (23)$$

As usual, we obtain the reference geometries $R_i^{j,ref}$ by first assuming their values to coincide with bond distances of the associated stationary points. Subsequently, we relax this condition via a trial-and-error least-squares fitting procedure. Similarly, the nonlinear range-determining parameters γ_i^j have been optimized in this way. The complete set of parameters amounts to a total of 171 coefficients c_i, 5 nonlinear coefficients γ_i^j, and 5 reference geometries $R_i^{j,ref}$. All numerical values of the least-squares parameters are gathered in Tables 4 and 5 of the Supporting Information. Table 3 shows the stratified root-mean-squared deviations (rmsd) values of the final PES with respect to all fitted ab-initio energies. A total of 809 points covering a range of energy up to ∼500 kcal mol^{-1} above the

dx.doi.org/10.1021/jp302173h | J. Phys. Chem. A 2012, 116, 4646–4656

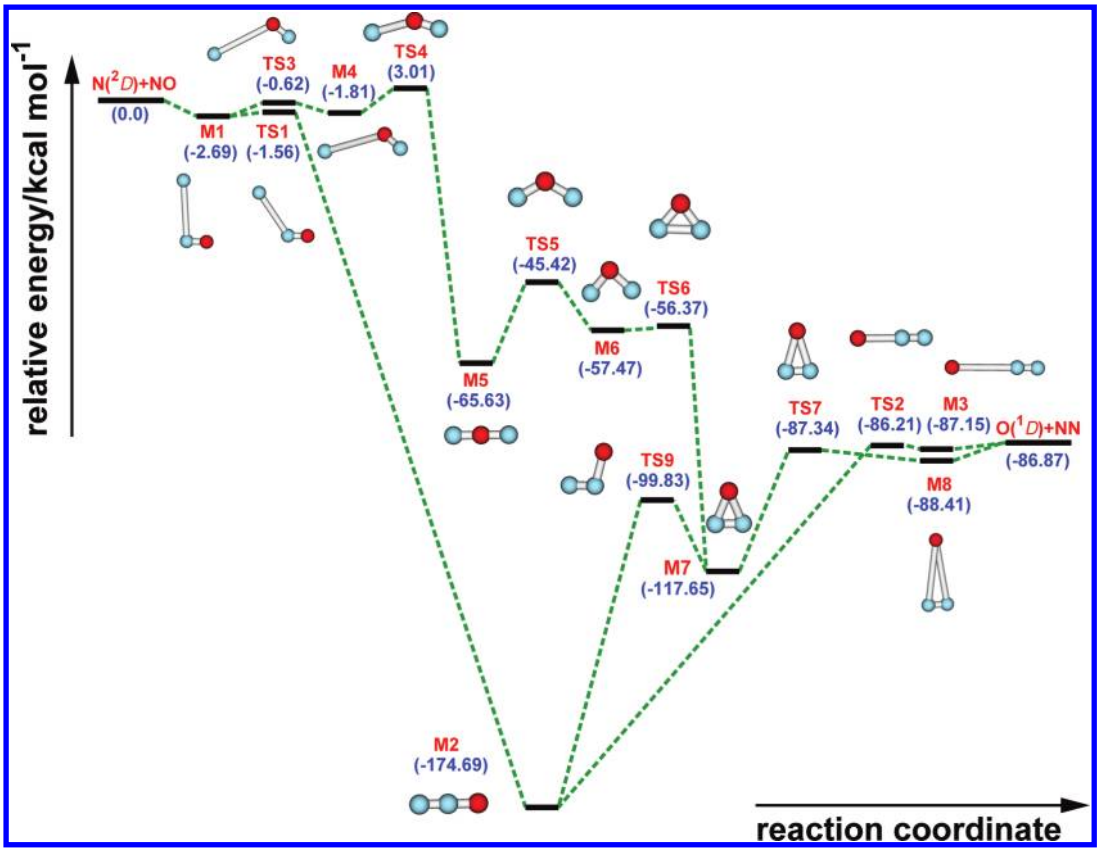

Figure 4. Energy diagram of stationary points located on the double many-body expansion (DMBE) PES. Energies (in kcal mol^{-1}) are relative to the N(^2D) + NO asymptote.

N_2O global minimum have been utilized for the calibration procedure, with the total rmsd being 0.940 kcal mol^{-1}.

4. FEATURES OF DMBE PES

Tables 4 and 5 compare the attributes of the stationary points of the DMBE PES with other theoretical and experimental results, having employed for the sake of comparison the labeling utilized in ref 15. In particular, we indicate the stationary-point geometries on the ground-state $^1A'$ PES that have been calculated through optimization searches of both minima (Ms) and transition states (TSs) at the MRCI(Q)/AVTZ level, employing analytic gradients. The results obtained by González et al.[15] at the CASPT2/6-311G(2d) level of theory and the analytical PES obtained from a fit to such points are also gathered in those two tables. The global minimum (M2) for the N_2O ground state is a linear (N−N−O) geometry in

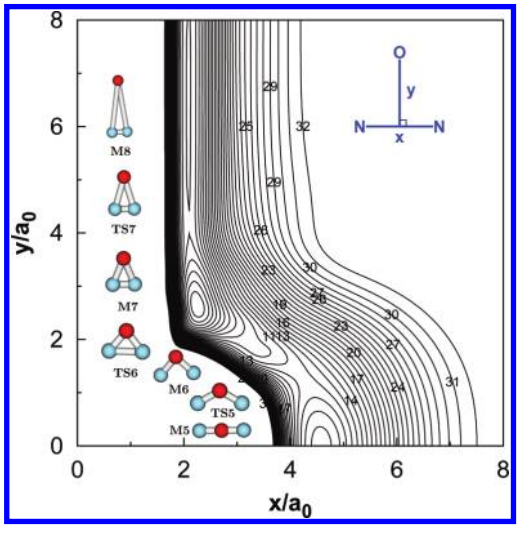

Figure 5. Contour plot for C_{2v} insertion of the O atom into the N_2 fragment. Contours equally spaced by 0.01 E_h, starting at −0.3427 E_h.

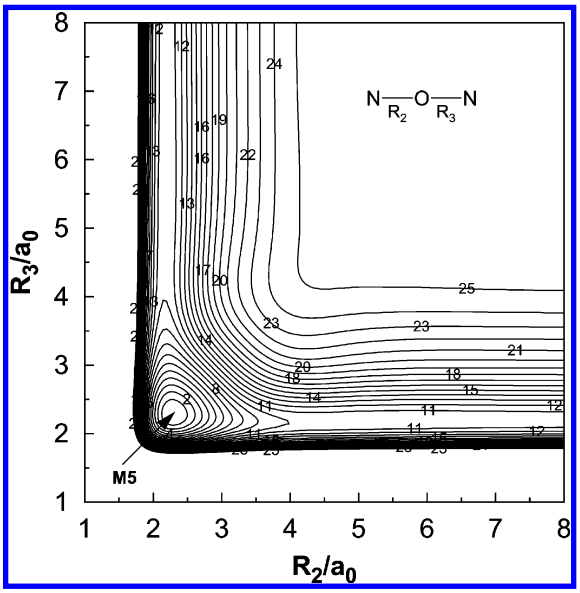

Figure 6. Contour plot for bond stretching in the N−O−N linear configuration. Contours equally spaced by 0.01 E_h, starting at −0.258 E_h.

dx.doi.org/10.1021/jp302173h | J. Phys. Chem. A 2012, 116, 4646−4656

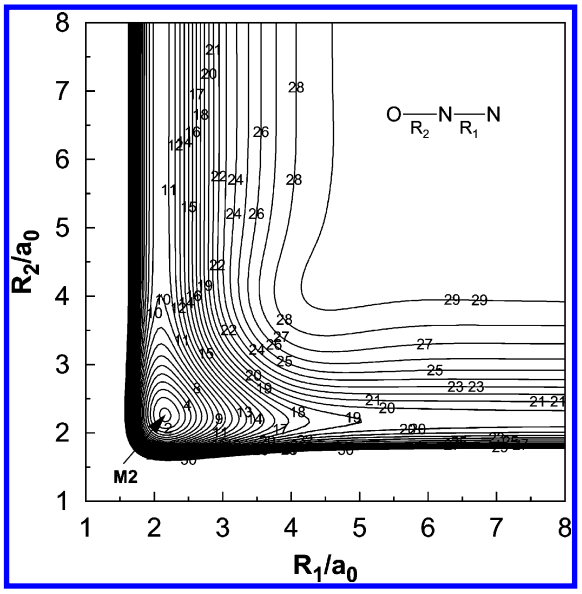

Figure 7. Contour plot for bond stretching in O−N−N collinear configuration. Contours equally spaced by 0.015 E_h, starting at −0.434 E_h.

our DMBE PES, which is predicated to be located at R_{NN} = 1.1399 Å and R_{NO} = 1.1928 Å and with a well depth of −174.69 and −89.63 kcal mol^{-1} relative to the $O(^1D)$ + $N_2(X^1\Sigma_g^+)$ and $N(^2D)$ + $NO(X\ ^2\Pi)$ dissociation energies, respectively. The energy differences with respect to the experimental data are 2.19 and 2.38 kcal mol^{-1}, relative errors less than 1.2% and 2.7%, respectively, in very good accordance with the experimental data. The existence of some of the reported minima has been noted previously; a linear NON minimum (M5) was confirmed and is well studied.[15,46,47] The present work yields for M5 a N−O distance of 1.2087 Å and a relative energy of −65.63 kcal mol^{-1}, in very good agreement with good-quality ab-initio data at the MRCI(Q)/AVTZ level of theory and other theoretical values. A cyclic-C_{2v} minimum (M7) in the ground state of N_2O is also reported in the present study as a more stable minimum than M5, with bond lengths of R_{NN} = 1.1891 Å and R_{NO} = 1.5145 Å and a relative energy of −117.65 kcal mol^{-1}. The above three isomers correspond therefore to a linear N−N−O structure as the global minimum with $C_{\infty v}$ symmetry, with the cyclic isomer having C_{2v} symmetry to be a local minimum lying 57.04 kcal mol^{-1} above the N−N−O global minimum and a linear N−O−N local minimum of $D_{\infty h}$ symmetry lying 109.06 kcal mol^{-1} higher than the global minimum and 52.02 kcal mol^{-1} above the cyclic C_{2v} one. Full agreement with other predictions is found insofar as the stability ordering of the three N_2O minima is concerned: NNO($C_{\infty v}$) > NON(C_{2v}) > NON($D_{\infty h}$). Many other minima and transition states found in the present work are also gathered in Tables 4 and 5 and compared with other theoretical predictions. As seen from Tables 4 and 5, the predicted values from our DMBE PES are in a good agreement with the stationary-point geometries obtained by optimization searches and other experimental and theoretical results.

In order to clarify the reactive mechanism, Figure 4 displays schematically the Ms and TSs predicted from the DMBE PES and their relative energies. Clearly, the reaction path is found to be in close agreement with previous work.[15] Several reactive paths can be distinguished from this plot. In the first path, the reacting $N(^2D)$ atom attacks the N end of the NO molecule (M1) and evolves through the transition state TS1 and global minimum M2, then proceeding via a linear barrier (TS2) and minimum (M3) before dissociating to the products (route 1). The second path also occurs via M1 but with the N atom attacking the O end of the NO molecule and hence forming structures with NON connectivity. It evolves through the transition state TS3 to form a bent van der Waals structure (M4) which connects to a linear $D_{\infty h}$ one (M5) through a transition state (TS4) with a barrier of 3.01 kcal mol^{-1} relative to the reactants. Keeping C_{2v} symmetry, the oxygen atom then moves away from NN through a series of minima (i.e., M6, M7,

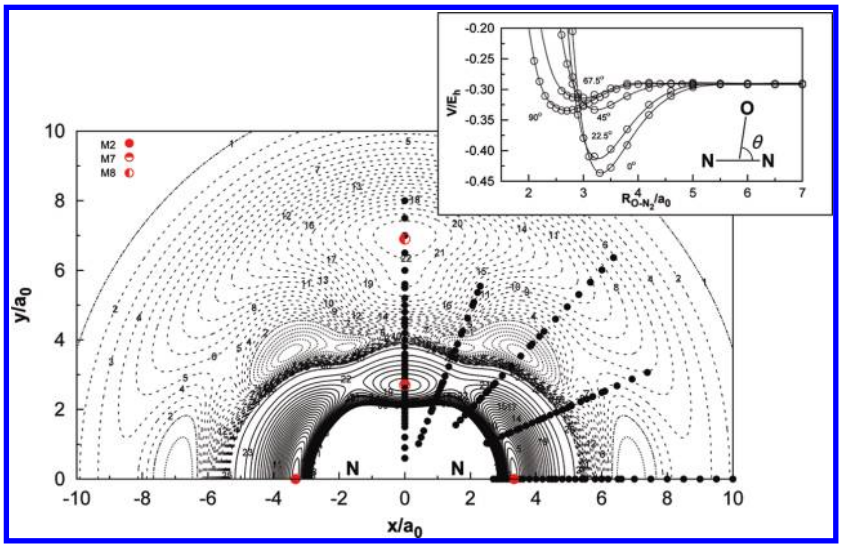

Figure 8. Contour plot for the O atom moving around a N_2 diatom fixed at its equilibrium geometry of R_{N_2} = 2.1410 a_0, which lies along the x axis with the center of the bond fixed at the origin. Contours are equally spaced by 0.006 E_h, starting at −0.4326 E_h. Dashed and dotted areas are contours equally spaced by −0.0001 and 0.0002 E_h, respectively, starting at −0.290 E_h. Also shown are the calculated ab-initio points for the O atom moving around N_2 diatomic, whose bond distance varied between 1.8 and 3.5 a_0. Shown at the insert are cuts along the atom−diatom radial coordinate for selected values of the Jacobi angle. Also indicated for clarity are the major minimal structures.

dx.doi.org/10.1021/jp302173h | J. Phys. Chem. A 2012, 116, 4646−4656

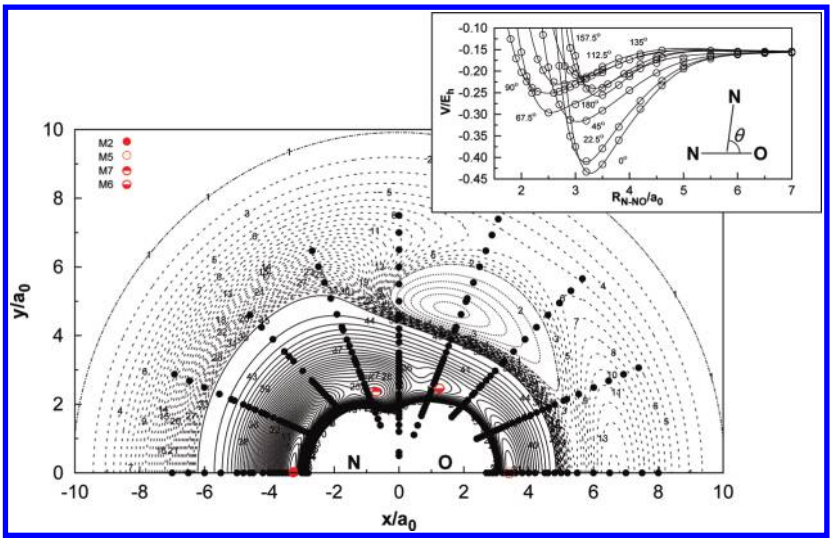

Figure 9. Contour plot for the N atom moving around a fixed NO diatom with the bond length fixed at R_{NO} = 2.2485 a_0, which lies along the x axis with the center of the bond fixed at the origin. Contours are equally spaced by 0.0062 E_h, starting at −0.4326 E_h. Dashed and dotted lines are contours equally spaced by −0.0002 and 0.001 E_h, respectively, starting at −0.15248 E_h. Also shown are the calculated ab-initio points for the N atom moving around NO diatomic, whose bond distance varied between 1.8 and 3.5 a_0. Insert shows cuts along the atom−diatom radial coordinate for selected values of the Jacobi angle. Minimal structures are also indicated for clarity.

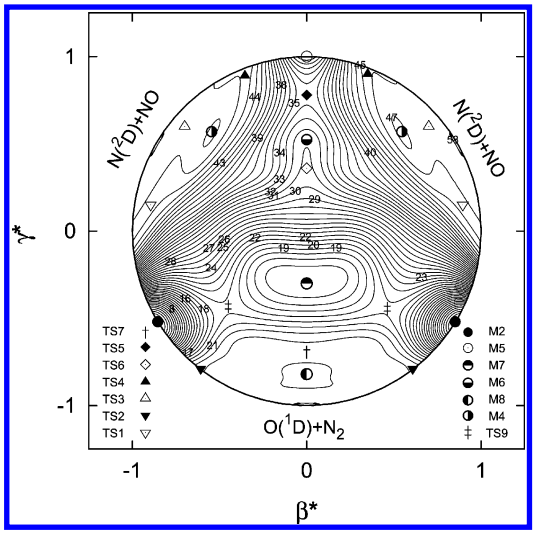

Figure 10. Relaxed triangular plot[49] in hyperspherical coordinates illustrating the location and symmetry of all stationary points discussed in the present work for ground-state N_2O.

and M8) and transition states (i.e., TS5, TS6 and TS7) before finally dissociating to products, $O(^1D)$ + $N_2(X^1\Sigma_g^+)$ (route 2). Connecting the above two paths, there is a C_s transition state, TS9. The third path starts in one of the above routes and ends on the other, forming $O(^1D)$ + $N_2(X^1\Sigma_g^+)$: it occurs through the global minimum (M2), transition state TS9 (with a barrier of 13.62 kcal mol^{-1} lower than TS2 in route 1), C_{2v} symmetry minimum M7, TS7 barrier, and minimum M8 to finally form the products (route 3).

Figures 5−9 show the major topographical features of the N_2O DMBE PES reported in the present work. The salient features from these plots are the most relevant stationary points for the title system, also characterized in Tables 4 and 5. As seen, all plots illustrate the smooth and correct behavior of the DMBE function for the ground-state N_2O species over its entire configuration space. In particular, Figure 5 shows a contour plot for the C_{2v} insertion of the $O(^1D)$ atom into N_2. It is visible from this plot that it reproduces the regions of the PES that link M8 and M5 through a series of transition states (i.e., TS7, TS6, and TS5) and minima (i.e., M7 and M6). When the O atom inserts into N_2, the ∠NON opens progressively while the distance of O to the center of N−N bond shortens and the bond length of N−N increases.

Figure 6 shows a contour plot for linear N−O−N stretch. The notable feature here is the linear N−O−N minimum (M5) located at R_{NO} = 1.2087 Å with an energy of 109.06 kcal mol^{-1} above of the global minimum of N_2O. In turn, Figure 7 illustrates in a clear manner the presence of the global minimum (M2). The predicted geometry is seen to agree nicely with the experimental results and with the PES reported by Schinke[18] which is based on MRCI calculations using the AVQZ basis set: the bond length differences are 0.0084 and 0.0031 Å, on the same order. The harmonic frequencies of the global minimum are 2253.3, 1314.1, and 453.6 cm^{-1}, with the MRCI(Q) results being 2283.9, 1298.8, and 600.3 cm^{-1}. In turn, the experimental values given by Warneck[48] are 2223.7, 1276.5, and 589.2 cm^{-1}, while the corresponding values reported by González et al.[15] at the CASPT2/6-311G(2d) level of theory and the analytical PES obtained from a fit to such points are 2223.7, 1269.6, and 589.5 cm^{-1} and 2216.3, 1250.2, and 589.7 cm^{-1} (respectively). As seen from Table 4, the results from the DMBE PES also show good agreement with the available estimates except, perhaps, for the bending frequency which is somewhat too small. Although this could possibly be improved by weigthing the points close to the minimum, no attempt has been made to do so since the experimental data refer to fundamentals rather than to harmonic frequencies.

Figure 8 shows a contour plot for the O atom moving around the N_2 ground-state diatom whose bond length is fixed at its equilibrium geometry of R_{NN} = 2.1410 a_0. The corresponding plot for the N atom moving around the NO diatom with its bond distance fixed at R_{NO} = 2.2485 a_0 is presented in Figure 9. The two plots clearly show a smooth behavior at both short- and long-range regions. From Figure 8 we can see the presence of minima (i.e., M2, M7, M8, M3) and transition states (i.e.,

TS7, TS9, TS2) according to dissociation routes 2 and 3 signaled above, see Figure 4. A transition state (TS9) is located between M2 and M7, corresponding basically to a stretched NNO structure which is located at R_{NN} = 1.1743 Å, R_{NO} = 1.4240 Å, and ∠NNO = 100.3° with an energy of 74.86 kcal mol^{-1} higher than the global minimum (M2) and 17.82 kcal mol^{-1} above M7. Also visible is the portion of the PES linking M8 to M7 minimum through the TS7 transition state, which corresponds to oxygen-atom insertion perpendicular to the N−N bond. Clearly, the trends mentioned when discussing Figure 4 are well reproduced. Also visible from this plot are TS2 and M3, which have linear geometries. Figure 9 shows the process connecting the linear ($C_{\infty v}$) NNO isomer to the cyclic (C_{2v}) and linear ($D_{\infty h}$) NON isomers, as indicated by M2 → TS9 → M7 → TS6 → M6 → TS5 → M5. In turn, Figures 8 and 9 illustrate the long-range parts of the PES which were fitted such as to provide a reliable description of the van der Waals minima and associated transition states.

All major topographical features of the PES are probably better viewed in a relaxed triangular plot[49] utilizing scaled hyperspherical coordinates ($\beta^* = \beta/Q$ and $\gamma^* = \gamma/Q$)

$$\begin{pmatrix} Q \\ \beta \\ \gamma \end{pmatrix} = \begin{pmatrix} 1 & 1 & 1 \\ 0 & \sqrt{3} & -\sqrt{3} \\ 2 & -1 & -1 \end{pmatrix} \begin{pmatrix} {R_1}^2 \\ {R_2}^2 \\ {R_3}^2 \end{pmatrix} \tag{24}$$

Figure 10 shows such a plot with all stationary points discussed above visible in it, thus allowing one to establish their connectivity in a more physical, multidimensional, way.

5. CONCLUDING REMARKS

A global single-sheeted DMBE PES has been reported for the ground state of N_2O from a least-squares fit to high-level AVTZ ab-initio energies, suitably corrected with the DMBE-SEC method. All topographical features have been carefully examined and compared with previously reported ones and experimental results when available. The DMBE PES here reported has been shown to be globally valid while fitting accurately all ab-initio points. A variety of minima and transition states has been predicted and various paths connecting reactants and products signaled. Good agreement is observed with previous high-quality theoretical studies and experimental data. The present single-sheeted DMBE PES should therefore be valuable for studying the dynamics and kinetics of reactions involving ground-state N_2O, work that is currently in progress.

■ ASSOCIATED CONTENT

Supporting Information

Parameters utilized to describe the DMBE potential-energy surface from this work and dispersion coefficients for the O−N_2 and N−NO channels as a function of the bond length of the diatomic. This material is available free of charge via the Internet at http://pubs.acs.org.

■ AUTHOR INFORMATION

Corresponding Author

*E-mail: varandas@qtvs1.qui.uc.pt.

Notes

The authors declare no competing financial interest.

■ ACKNOWLEDGMENTS

This work was financed by FEDER through Programa Operacional Factores de Competitividade-COMPETE and national funds under the auspices of Fundação para a Ciência e a Tecnologia, Portugal (projects PTDC/QUI-QUI/099744/2008, PTDC/AAC-AMB/099737/2008, and SFRH/BD/66471/2009).

■ REFERENCES

(1) Ravishankara, A. R.; Daniel, J. S.; Portmann, R. W. *Science* **2009**, *326*, 123.
(2) Remsen, L. G.; Pagel, M. A.; McCormick, C. I.; Fiamengo, S. A.; Sexton, G.; Neuwelt, E. A. *Anesth. Analg. (N.Y.)* **1999**, *88*, 559.
(3) Alm, J.; Saarnio, S.; Nykanen, H.; Silvola, J.; Martikainen, P. J. *Biogeochemistry* **1999**, *44*, 163.
(4) Rahn, T.; Zhang, H.; Wahlen, M.; Blake, G. A. *Res. Lett.* **1998**, *25*, 1189.
(5) Chakraborty, D.; Lin, M. C. *J. Phys. Chem. A* **1999**, *103*, 601.
(6) Maki, A. G.; Wells, J. S.; Vanek, M. D. *J. Mol. Spectrosc.* **1989**, *138*, 84.
(7) Teffo, J.-L.; Chendin, A. *J. Mol. Spectrosc.* **1989**, *135*, 389.
(8) Hishikawa, A.; Iwamae, A.; Hoshina, K.; Kono, M.; Yamanouchi, K. *Res. Chem. Intermed.* **1998**, *24*, 765.
(9) Brown, A.; Jimeno, P.; Balint-Kurti, G. G. *J. Phys. Chem. A* **1999**, *103*, 11089.
(10) Johnson, M. S.; Billing, G. D.; Gruodis, A.; Janssen, M. H. M. *J. Phys. Chem. A* **2001**, *105*, 8672.
(11) Nakamura, H.; Kato, S. *J. Chem. Phys.* **1999**, *110*, 9937.
(12) Varandas, A. J. C. *Adv. Chem. Phys.* **1988**, *74*, 255.
(13) Varandas, A. J. C. In *Lecture Notes in Chemistry*; Laganá Riganelli, A., Ed.; Springer: Berlin, 2000; Vol. 75, pp 33.
(14) Varandas, A. J. C. *Conical Intersections: Electronic Structure, Spectroscopy and Dynamics*; Advanced Series in Physical Chemistry; World Scientific Publishing: Singapore, 2004; Chapter 5, p 91.
(15) González, M.; Valero, R.; Sayós, R. *J. Chem. Phys.* **2000**, *113*, 10983.
(16) Daud, M. N.; Balint-Kurti, G. G.; Brown, A. *J. Chem. Phys.* **2005**, *122*, 054305.
(17) Nanbu, S.; Johnson, M. S. *J. Phys. Chem. A* **2004**, *108*, 8905.
(18) Schinke, R. *J. Chem. Phys.* **2011**, *134*, 064313.
(19) Defazio, P.; Gamallo, P.; Petrongolo, C. *J. Chem. Phys.* **2012**, *136*, 054308.
(20) Werner, H. J.; Knowles, P. J. *J. Chem. Phys.* **1988**, *89*, 5803.
(21) Knowles, P. J.; Werner, H.-J. *Chem. Phys. Lett.* **1985**, *115*, 259.
(22) Marchetti, O.; Werner, H.-J. *Phys. Chem. Chem. Phys.* **2008**, *10*, 3400.
(23) Dunning, T. H., Jr. *J. Chem. Phys.* **1989**, *90*, 1007.
(24) Varandas, A. J. C. *J. Chem. Phys.* **1989**, *90*, 4379.
(25) Werner, H.-J.; Knowles, P. J.; Knizia, G.; Manby, F. R.; Schütz, M.; et al. *MOLPRO*, version 2010.1, a package of ab initio programs; University College Cardiff: Cardiff, UK, 2010.
(26) Murrell, J. N.; Carter, S. *J. Phys. Chem.* **1984**, *88*, 4887.
(27) Varandas, A. J. C.; Poveda, L. A. *Theor. Chem. Acc.* **2006**, *116*, 404.
(28) Varandas, A. J. C. *J. Chem. Phys.* **1996**, *105*, 3524.
(29) Varandas, A. J. C.; Silva, J. D. *J. Chem. Soc., Faraday Trans.* **1992**, *88*, 941.
(30) Varandas, A. J. C. *Mol. Phys.* **1987**, *60*, 527.
(31) Huber, K. P.; Herzberg, G. *Molecular Spectra and Molecular Structure Constants of Diatomic Molecules*; van Nostrand Reinhold: New York, 1979.
(32) Lodders, K. *J. Phys. Chem. Ref. Data.* **2004**, *33*, 357.
(33) Brown, F. B.; Truhlar, D. G. *Chem. Phys. Lett.* **1985**, *117*, 307.
(34) Varandas, A. J. C. *Chem. Phys. Lett.* **1992**, *194*, 333.
(35) Martnez-Núñez, E.; Varandas, A. J. C. *J. Phys. Chem. A* **2001**, *105*, 5923.
(36) Rodrigues, S. P. J; Sabn, J. A.; Varandas, A. J. C. *J. Phys. Chem. A* **2002**, *106*, 556.

(37) Varandas, A. J. C.; Rodrigues, S. P. J *J. Phys. Chem A* **006**, *110*, 485.
(38) Varandas, A. J. C.; Rodrigues, S. P. J *J. Phy. Chem. A* **2007**, *111*, 4869.
(39) Varandas, A. J. C. *J. Mol. Struct. (THEOCHEM)* **1988**, *166*, 59.
(40) Varandas, A. J. C.; Brandão, J.; Quintales, L. A. M. *J. Phys. Chem.* **1988**, *92*, 3723.
(41) Varandas, A. J. C.; C., A. A. C. *Pais, Mol. Phys.* **1988**, *65*, 843.
(42) Varandas, A. J. C.; Rodrigues, S. P. J *J. Chem. Phys.* **1997**, *106*, 9647.
(43) Rodrigues, S. P. J; Varandas, A. J. C. *Phys. Chem. Chem. Phys.* **2000**, *2*, 435.
(44) Varandas, A. J. C. In *Conferencias Plenarias de la XXIII Reunión Bienal de Qumica*; Feliciano, A. S., Grande, M., Casado, J., Eds.; Universidad de Salamanca: Salamanca, 1991; p 321.
(45) Martínez-Nuñez, E.; Varandas, A. J. C. *J. Phys. Chem.* **2001**, *105*, 5923.
(46) Peyerimhoff, S. D.; Buenker, R. J. *J. Chem. Phys.* **1968**, *49*, 2473.
(47) Wang, F.; Harcourt, R. D. *J. Phys. Chem. A* **2000**, *104*, 1304.
(48) Warneck, P. *Chemistry of the Natural Atmosphere*; Academic: San Diego, 1998.
(49) Varandas, A. J. C. *Chem. Phys. Lett.* **1987**, *138*, 455.
(50) Huber, K. P.; Herzberg, G. *Molecular Spectra and Molecular Structure. IV Constants of Diatomic Molecules*; Van Nostrand: New York, 1979.
(51) Bashkin, S.; Stoner, J. O., Jr. *Atomic Energy Levels and Grotrian Diagrams*; North-Holland: Amsterdam, 1975.